Lung Cancer 219 (2026) 109553

Contents lists available at ScienceDirect

Lung Cancer

journal homepage: www.elsevier.com/locate/lungcan

Research Paper

# Low baseline cGAS expression is associated with longer progression-free survival in patients with pleural mesothelioma

Antoine Torchiat [a], Karina Silina [b], Arya Ashok Nair [a], Laura Viktoria Heeb [a], Isabelle Opitz [c], Anurag Gupta [a], Alessandra Curioni-Fontecedro [a,*]

[a] Department of Medical and Surgical Specialties, Faculty of Science and Medicine, University of Fribourg, Fribourg, Switzerland
[b] ETH Zurich, Zurich, Switzerland
[c] Department of Thoracic Surgery, University Hospital Zurich, Zurich, Switzerland

ARTICLE INFO

*Keywords:*
cGAS
STING
Pleural mesothelioma
Multiparameter immunofluorescence

ABSTRACT

*Introduction:* The cyclic GMP-AMP synthase (cGAS)/STING pathway, a central DNA-sensing mechanism, is known to activate anti-tumor immune response but may also promote tumor progression when chronically activated. Given the role of asbestos-induced chronic inflammation in pleural mesothelioma (PM), we investigated cGAS/STING expression and its association with treatment outcomes.

*Methods:* We analyzed tissue microarrays from 190 PM patients using multiparameter immunofluorescence single-cell imaging. cGAS and STING expression were quantified in Calretinin$^+$ tumor cells, Calretinin$^-$CD8$^-$DC-LAMP$^-$ cells, and CD8$^+$ cells before and after chemotherapy. Associations with treatment response and survival were assessed.

*Results:* In matched pre- and post-treatment samples, total cGAS$^+$ cell frequency increased after chemotherapy, as did cGAS$^+$ frequencies in Calretinin$^+$ tumor cells, Calretinin$^-$CD8$^-$DC-LAMP$^-$ cells, and CD8$^+$ cells after FDR correction, whereas STING$^+$ cell frequency did not differ. Within the progressive-disease subgroup, significant paired increases were retained for total cGAS$^+$ cells and Calretinin$^-$CD8$^-$DC-LAMP$^-$ cells. However, the magnitude of change did not differ significantly among patients with partial response, stable disease, or progressive disease. Low baseline total cGAS$^+$ frequency and cGAS$^+$ frequency in Calretinin$^-$CD8$^-$DC-LAMP$^-$ cells were associated with longer progression-free survival. In an exploratory analysis of the TCGA PM cohort, higher CGAS/MB21D1 transcript expression was associated with shorter overall survival in continuous Cox regression, whereas STING1 transcript expression was not significantly associated with overall survival when analyzed as a continuous variable.

*Conclusions:* Low baseline cGAS$^+$ frequency, particularly in the Calretinin$^-$CD8$^-$DC-LAMP$^-$ compartment, was associated with longer progression-free survival in PM. These findings support further evaluation of cGAS as a candidate prognostic biomarker but do not establish cGAS as a predictor of chemotherapy response or as a causal driver of treatment resistance.

## Introduction

Pleural mesothelioma (PM) is an aggressive malignancy of the pleural lining, predominantly caused by asbestos exposure. Inhaled asbestos fibers accumulate in the visceral pleura, acting as a persistent stimulus for chronic inflammation [1]. Despite multimodal therapies, prognosis remains poor. In 2020, the combination of the immune checkpoint inhibitors ipilimumab (anti–CTLA-4) and nivolumab

*Abbreviations:* AMP, adenosine monophosphate; AMPK, 5′ AMP-activated protein kinase; cGAMP, cyclic guanosine monophosphate–adenosine monophosphate; cGAS, cyclic GMP-AMP synthase; DC, dendritic cell; FFPE, formalin-fixed paraffin-embedded; GMP, guanosine monophosphate; HR, hazard ratio; IDO, indoleamine 2,3 dioxygenase; IRF3, interferon regulatory factor 3; MDSC, myeloid-derived suppressor cell; OS, overall survival; PD, progressive disease; PFS, progression-free survival; PM, pleural mesothelioma; PR, partial response; ROS, reactive oxygen species; SD, stable disease; STING, stimulator of interferon genes; TBK1, TANK-binding kinase 1; TCGA, the cancer genome atlas; TMA, tissue microarray.

* Corresponding author at: Head of Oncology, Cantonal Hospital Fribourg University of Fribourg, Department of Medical and Surgical Specialties, Faculty of Science and Medicine, Chemin du Museé 18, 1700, Fribourg, Switzerland

*E-mail address:* Alessandra.Curioni-Fontecedro@h-fr.ch (A. Curioni-Fontecedro).

https://doi.org/10.1016/j.lungcan.2026.109553
Received 7 May 2026; Received in revised form 20 July 2026; Accepted 26 July 2026
Available online 28 July 2026

(anti–PD-1) was approved, showing only modest benefit—a median overall survival (OS) gain of four months compared with platinum-based chemotherapy [2,3]. These limited improvements may be due to the low immunogenicity of mesothelioma, the presence of an immunosuppressive tumor microenvironment, and ineffective anti-tumor immune responses. Understanding the molecular and immunological biology of PM is therefore critical for developing new therapeutic strategies.

The cyclic GMP–AMP synthase (cGAS) and its downstream effector, stimulator of interferon genes (STING), are central components of the cytosolic DNA sensing pathway [4]. Upon binding cytosolic double-stranded DNA—derived from viral infection, genomic instability, or DNA damage—cGAS produces cyclic GMP–AMP (cGAMP), which activates STING. Activated STING recruits and phosphorylates interferon regulatory factor 3 (IRF3), inducing type I interferons and other immune-related genes [5]. Type I interferons are essential for T cell priming and effective anti-tumor immunity. Preclinical studies show that STING agonists enhance anti-tumor immunity and promote tumor regression through type I interferon production [6,7]. In addition, genotoxic chemotherapies induce DNA damage and activate the cGAS/STING pathway, facilitating CD8 + cell infiltration and improving responses to chemotherapy and checkpoint blockade [8].

However, growing evidence indicates that the cGAS/STING pathway may also promote tumor progression. STING activation can recruit myeloid-derived suppressor cells (MDSCs) [9], upregulate immune checkpoint molecules such as PD-L1 − an interferon-response gene indirectly induced through the STING–type I IFN axis and IDO [10], and, when chronically stimulated, drive metastasis through induction of epithelial–mesenchymal transition [10,11] and maintenance of cancer stemness [12]. Furthermore, nuclear cGAS has been shown to inhibit homologous recombination-mediated DNA repair, thereby promoting genomic instability and tumorigenesis [13].

Given the role of chronic inflammation in mesothelioma pathogenesis, we hypothesized that aberrant cGAS/STING activation contributes to tumor progression and treatment outcomes in PM. To test this, we analyzed cGAS and STING expression in mesothelioma tumor cells and infiltrating immune cells using tissue microarrays (TMAs) from matched pre- and post-chemotherapy samples.

## Material and methods

### *Patient samples*

Tumor tissues were collected from 190 patients with PM treated at the University Hospital Zurich between 1999 and 2009, as described previously [14]. Samples were obtained before the start of chemotherapy (pre-treatment) and after three cycles of platinum-based chemotherapy combined with either gemcitabine or pemetrexed (post-treatment). All patients provided written informed consent, and the study was approved by the Cantonal Ethics Committee of Zurich (reference number EK-ZH 2020-02566), in accordance with the Declaration of Helsinki.

### Tissue microarrays (TMAs)

Formalin-fixed paraffin-embedded (FFPE) samples were retrieved from the Institute of Pathology and Molecular Pathology, University Hospital Zurich. TMAs were constructed using a semi-automatic tissue arrayer (Beecher Instruments), with at least two punches per case (core diameter 0.6 mm), as described [14].

### Multiparameter immunofluorescence (mIF)

TMAs were analyzed by mIF to characterize immune and tumor populations. FFPE sections (4 μm) were processed in Trilogy™ buffer (CellMarque) for 90 min at 95 °C, blocked with 4% bovine serum albumin/PBS/0.1% Triton X, and sequentially stained with antibodies against cGAS (D1D3G, Cell Signaling, 1:500), DC-LAMP (1010E1.01, Dendritics, 1:1000), Calretinin (SP13, Origene, 1:200), CD8 (4B11, Bio-Rad, 1:1000), STING (D2P2F, Cell Signaling, 1:500), CD4 (MSVA-004R, Cell Signaling, 1:100), CD11b (D6X1N, Cell signaling, 1:100) and CD68 (D4B9C, Cell signaling, 1:300). HRP-conjugated secondary antibodies (Jackson ImmunoResearch, minimal cross-reactivity) and the 7-plex Opal system (Akoya) were used for detection, followed by DAPI nuclear counterstaining (SIGMA) and mounting with Prolong Diamond antifade reagent (Thermo Scientific).

### Quantitative image analysis

Each TMA core was imaged at 200 × magnification using the Vectra 3.0 multispectral microscope (PerkinElmer/Akoya). Image analysis included: (1) spectral unmixing, (2) single-cell segmentation, and (3) extraction of per-cell fluorescence intensities using Inform software v2.4. Files were converted to flow cytometry format using Biobase and flowCore (15) R packages and analyzed in FlowJo v10.8.0. Marker-defined populations consisted of $CD8^+$ cells, DC-$LAMP^+$ cells, Calretinin$^+$CD8$^-$DC-LAMP$^-$ tumor cells, and Calretinin$^-$CD8$^-$DC-LAMP$^-$ unclassified non-tumor cells. cGAS and STING expression was quantified within each population (**Fig. S1a–d**). In addition, separately not as part of the 7-plex Opal system, we stained for CD4, CD11b, CD68 to quantify the cells in TMAs (**Fig. S2**).

### Quality control and statistics

Cores with < 500 cells, tissue damage, or staining artifacts were excluded. To account for intratumoral heterogeneity, the mean of at least two tumor cores per patient was used. Statistical analyses were performed in R v4.5.1. Pre- and post-treatment comparisons were performed separately within the biphasic and epithelioid histological subtypes using paired Wilcoxon signed-rank tests. The ten prespecified paired pre- and post-treatment comparisons presented across all the data were adjusted together within the epithelioid cases and separately within the biphasic cases using the Benjamini–Hochberg procedure. Comparisons between biphasic and epithelioid tumors at the pre-treatment and post-treatment time points were performed using Wilcoxon rank-sum tests and were adjusted as a separate family using the Benjamini–Hochberg procedure. For paired pre- and post-treatment comparisons within each response group were performed using Wilcoxon signed-rank tests, with Benjamini–Hochberg correction across the prespecified paired comparisons. Changes in cell-population frequencies, calculated as post-treatment minus pre-treatment values, were compared across response groups using Kruskal–Wallis tests with Benjamini–Hochberg FDR correction. Pairwise Wilcoxon rank-sum tests were planned only following a significant omnibus Kruskal–Wallis test. Because none of the omnibus tests was significant, no post-hoc pairwise comparisons were performed. DC-LAMP + cells were excluded from downstream analysis due to low abundance. FDR-adjusted p-values are reported. Significance was indicated as ****FDR-adjusted $p < 0.0001$, ***FDR-adjusted $p < 0.001$, **FDR-adjusted $p < 0.01$, and *FDR-adjusted $p < 0.05$.

### Survival analysis

Progression-free survival (PFS) was defined from treatment initiation to documented progression. Kaplan–Meier analyses were performed using the evaluate Cutpoints R package [15,16] to determine optimal cutoffs (CutP method). Survival curves, hazard ratios, and risk tables were generated with the survival and survminer R packages [17]. Statistical significance was assessed by log-rank test, with $p < 0.05$ considered significant. Univariate Cox proportional hazards models were fitted to assess the association between baseline cGAS$^+$ cell frequencies and PFS, and between CGAS/MB21D1 or STING1 transcript expression and OS, with predictors analyzed as continuous variables.

Hazard ratios corresponded to a one-unit increase in the respective continuous variable. The proportional hazards assumption was assessed using Schoenfeld residuals.

### TCGA cohort

Batch-normalized RNA-sequencing expression data for CGAS/MB21D1 and STING1, together with overall survival data, were downloaded from cBioPortal for the TCGA PanCancer Atlas mesothelioma cohort (study ID: meso_tcga_pan_can_atlas_2018; accessed July 14, 2026). Analyses included 86 chemotherapy-naïve patients with complete expression and survival data. mRNA expression was quantified as batch-normalized RSEM values from Illumina HiSeq RNASeqV2. Kaplan–Meier and continuous univariate Cox proportional hazards analyses were performed as described above.

## Results

### *PM patient cohort*

The clinicopathological characteristics of the pleural mesothelioma (PM) cohort (n = 190) are summarized in Table 1 [14]. The median patient age was 61 years (range 35–81), and the majority were male (170, 89%). Histological subtypes included 124 epithelioid (65%), 56 biphasic (30%), 6 sarcomatoid (3%), and 4 unknown (2%). Treatments comprised cisplatin in 150 patients (79%), pemetrexed in 93 (47%), gemcitabine in 62 (33%), and carboplatin in 16 (8%). Clinical responses included partial response (PR) in 29 patients (15%), stable disease (SD) in 46 (24%), progressive disease (PD) in 27 (14%), while 88 (46%) had unknown response status. Median progression-free survival (PFS) from treatment initiation was 16.1 months (range 0.5–140.3), and median overall survival (OS) was 24.2 months (range 0.5–140.3). Quality-controlled TMAs contained tumor samples from 130 patients before chemotherapy and 122 patients after chemotherapy (**Fig. S3a**). Among these, 72 patients had matched pre- and post-treatment samples that were used for longitudinal analysis. The distribution of analyzed samples according to histological subtype is shown in **Fig. S3b**. Due to the limited number of sarcomatoid cases, only three matched cases passed quality control. These cases were excluded from the primary histological-subtype analyses and were examined separately in an analysis presented in **Fig. S4**. Thus, data from epithelioid and biphasic histotypes are shown in the primary analyses. Treatment-response and survival data were available for 56 patients, who were included in the outcome analyses (**Fig. S3a**).

**Table 1**
Clinicopathological characteristics of the global cohort [cases (n = 190)].

| Characteristic | | N = 190 |
|---|---|---|
| Age median (range) (ys) | | 61 (35—81) |
| Sex, n (%) | | |
| | Men | 170 (89.47) |
| | Women | 20 (10.53) |
| Histological subtype, n (%) | | |
| | Epithelioid | 124 (65.26) |
| | Biphasic | 56 (29.47) |
| | Sarcomatoid | 6 (3.16) |
| | NA | 4 (2.11) |
| Treatment, n (%) | | |
| | Cisplatin | 150 (78.95) |
| | Pemetrexed | 93 (46.84) |
| | Gemcitabine | 62 (32.63) |
| | Carboplatin | 16 (8.42) |
| Response | | |
| | PR | 29 (15.26) |
| | SD | 46 (24.21) |
| | PD | 27 (14.21) |
| | NA | 88 (46.32) |
| OS median (range) (month) | | 24.17 (0.46—140.28) |
| PFS median (range) (month) | | 16.06 (0.46—140.28) |
| Time of sample collection | | |
| | Pre chemotherapy | 130 |
| | Post chemotherapy | 122 |
| | no chemotherapy | 8 |
| | matching | 72 |

### Chemotherapy induces cGAS expression

Expression of cGAS, Calretinin, STING, CD8, and DC-LAMP were evaluated by multiparameter immunofluorescence and multispectral microscopy on PM tumor tissue microarrays (TMAs) (Fig. 1). Based on marker expression, we defined the following cell populations: $CD8^+$ cells ($CD8^+$), tumor cells ($Calretinin^+$, $CD8^-$, $DC\text{-}LAMP^-$), $DC\text{-}LAMP^+$ cells, and non-tumor cells ($CD8^-$, $Calretinin^-$, $DC\text{-}LAMP^-$). Cells were further gated for cGAS and STING expression (**Fig. S1a–d**). Expression was compared between pre- and post-chemotherapy samples (Fig. 2). $DC\text{-}LAMP^+$ cells were excluded from downstream analyses because of their very low frequencies (<0.2% of all cells) across the samples. When analyzed, we noticed substantially low number of CD4, CD11b and CD68 cells in TMAs (Fig. S2); thus, these cells were excluded from any further analysis. The frequency of $Calretinin^+$ tumor cells did not change after chemotherapy for any of the evaluated histological subtypes (**Fig. S3a**).

Paired pre- and post-treatment analyses were performed separately within biphasic and epithelioid tumors. Total $cGAS^+$ cell frequency increased after chemotherapy in both biphasic and epithelioid tumors (FDR-adjusted p = 0.0005 and 0.0002, respectively), whereas $STING^+$ cell frequency did not differ in either subtype (FDR-adjusted p = 0.589 and 0.839, respectively) (Fig. 2**a,b**). The frequency of $cGAS^+STING^+$ cells increased in both biphasic and epithelioid tumors (FDR-adjusted p = 0.00091 and 0.00266, respectively) (Fig. 2**c**). Increased $cGAS^+$ frequencies were also observed in $Calretinin^+$ tumor cells (FDR-adjusted p = 0.00236 and 0.00162), $Calretinin^-CD8^-DC\text{-}LAMP^-$ cells (FDR-adjusted p = 0.00047 and 0.00162), and $CD8^+$ cells (FDR-adjusted p = 0.00236 and 0.00565) in biphasic and epithelioid tumors, respectively (Fig. 2**d–f**). At baseline, cGAS + frequency in Calretinin + tumor cells differed significantly between biphasic and epithelioid tumors after FDR correction (FDR-adjusted p = 0.048; Fig. 2**d**).

The frequency of $Calretinin^+$ tumor cells did not differ significantly after chemotherapy in either biphasic or epithelioid tumors (FDR-adjusted p = 0.483 and 0.304, respectively; **Fig. S5a**). In contrast, $cGAS^+STING^+$ frequency in $Calretinin^-CD8^-DC\text{-}LAMP^-$ cells increased in both subtypes (FDR-adjusted p = 0.00108 and 0.00556, respectively; **Fig. S5b**). Overall $CD8^+$ cell frequency also increased in biphasic and epithelioid tumors (FDR-adjusted p = 0.0416 and 0.0226, respectively; **Fig. S5c**), as did $cGAS^+STING^+$ $CD8^+$ cell frequency (FDR-adjusted p = 0.0213 and 0.0216, respectively; **Fig. S5d**).

### Chemotherapy-associated changes in $cGAS^+$ cell frequencies across response groups

We next examined paired pre- and post-treatment $cGAS^+$ cell frequencies within each response group. After FDR correction, a significant increase in total $cGAS^+$ cell frequency was observed within the progressive-disease group, but not the partial-response or stable-disease groups (FDR-adjusted p = 0.032; Fig. 3**a**). No significant paired changes were observed in $Calretinin^+$ tumor cells or $CD8^+$ cells (Fig. 3**b,d**). In the $Calretinin^-CD8^-DC\text{-}LAMP^-$ compartment, a significant increase was observed again within the progressive-disease group (FDR-adjusted p = 0.041; Fig. 3**c**).

We then compared changes in $cGAS^+$ cell frequencies, calculated as post-treatment minus pre-treatment values, among the PR, SD, and PD groups. No significant differences were observed among response groups for total $cGAS^+$ cells, $Calretinin^+$ tumor cells, Calretinin − CD8 − DC-LAMP − cells, or CD8 + cells after FDR correction (all FDR-adjusted p ≥ 0.92; Fig. 3**e–h**). Because none of the omnibus Kruskal–Wallis tests was

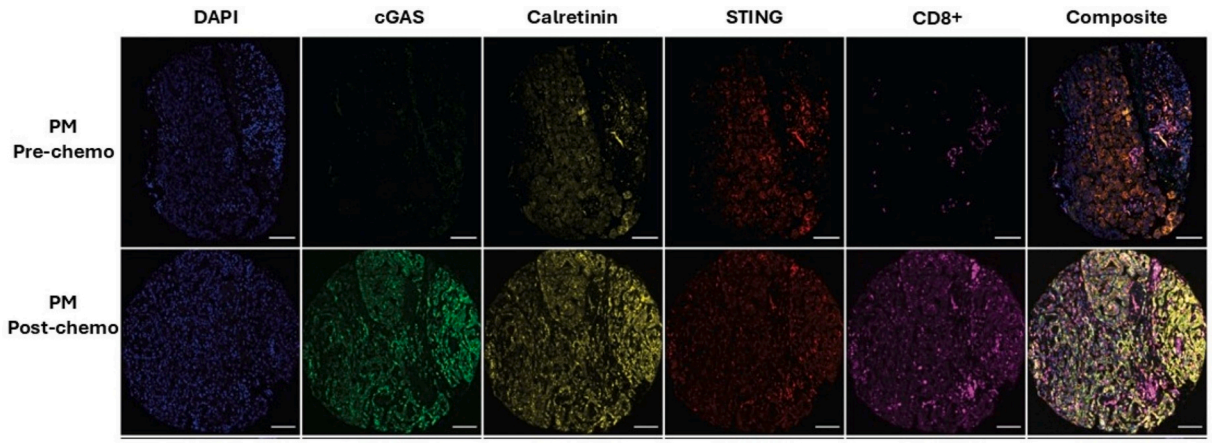


**Fig. 1.** Representative TMA cores from MPM tumors pre- and post-chemotherapy treatment: TMAs were stained for DAPI (blue), cGAS (green), Calretinin (yellow), STING (red) and CD8 (purple). 100 μm scale bars.

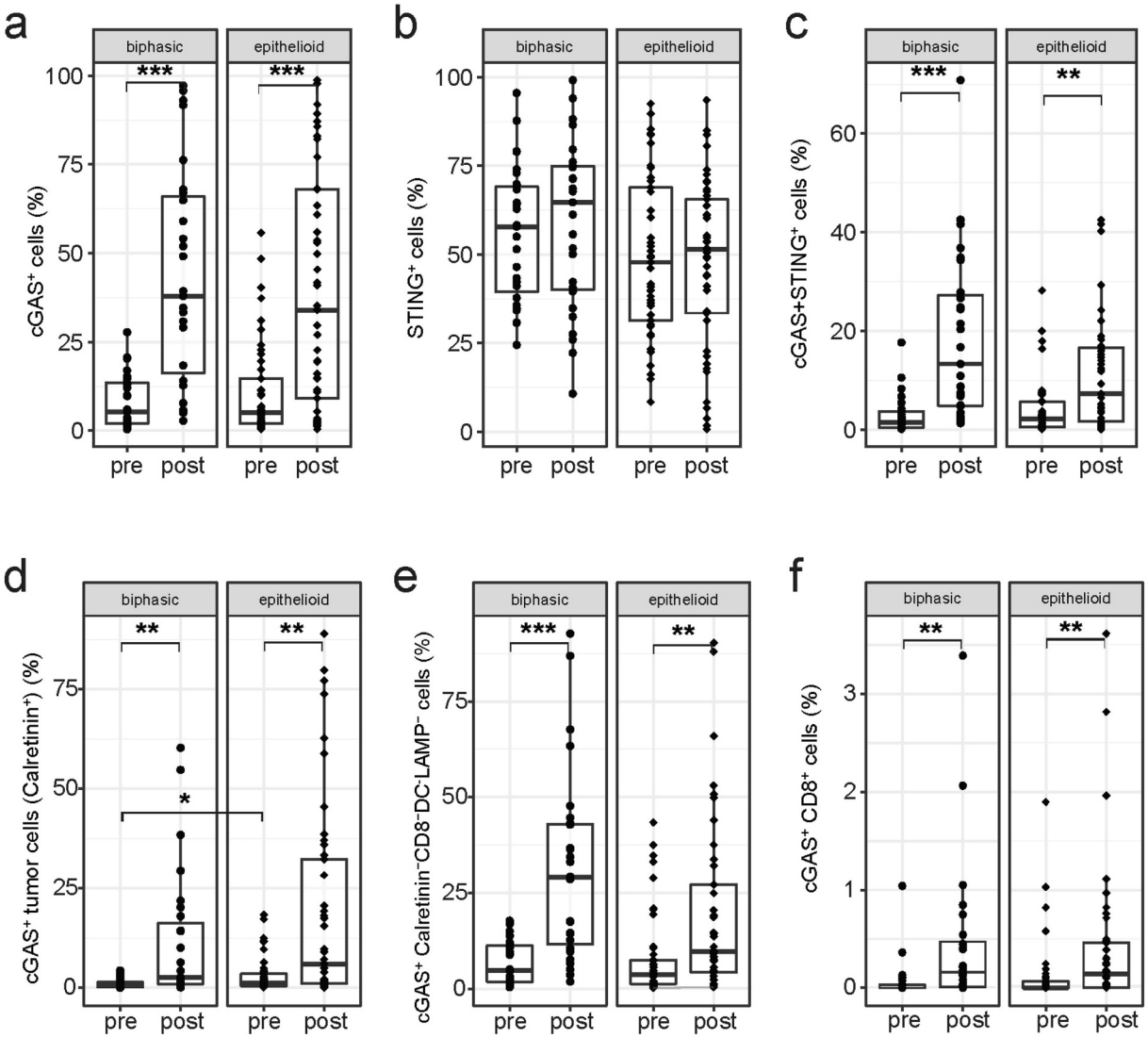


**Fig. 2.** Expression of cGAS and STING in different cell subtypes quantified on a single cell level before and after chemotherapy. Frequencies are shown for (a) total cGAS$^+$ cells, (b) total STING$^+$ cells, (c) cGAS$^+$STING$^+$ cells, (d) cGAS$^+$ Calretinin$^+$ tumor cells, (e) cGAS$^+$ Calretinin$^-$CD8$^-$DC-LAMP$^-$ cells, and (f) cGAS$^+$ CD8$^+$ cells. All frequencies are expressed as percentages of total segmented cells. Pre- and post-treatment comparisons were performed separately within the biphasic and epithelioid histological subtypes using paired Wilcoxon signed-rank tests. Benjamini–Hochberg false discovery rate correction was applied across the ten prespecified paired comparisons presented in Figs. 2 and S3, separately within each histological subtype. Comparisons between biphasic and epithelioid tumors at each time point were performed using Wilcoxon rank-sum tests and adjusted as a separate family using the Benjamini–Hochberg procedure.

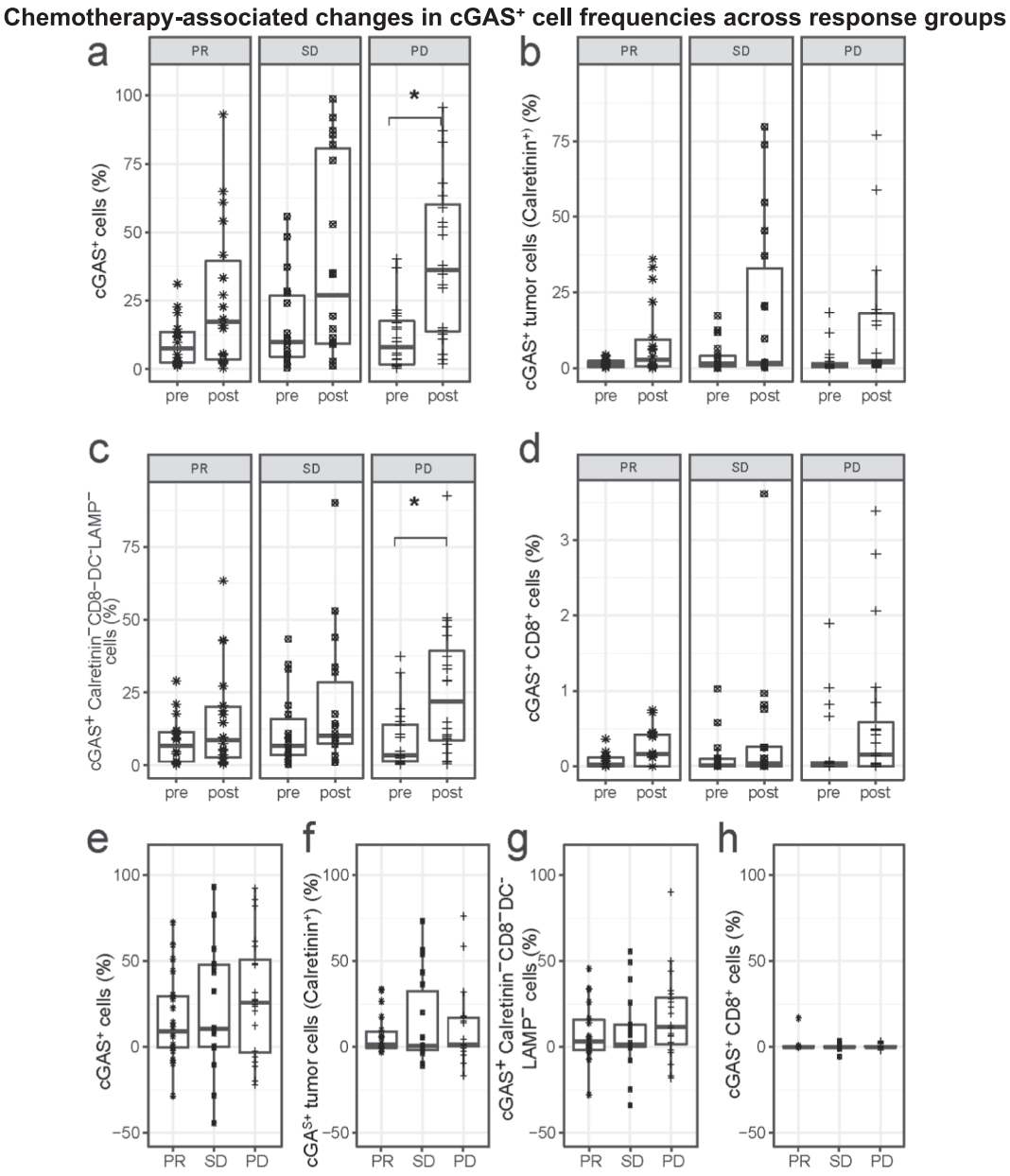


**Fig. 3.** Changes in cGAS$^+$ cell frequencies according to chemotherapy response. Data from epithelioid and biphasic cases were combined and grouped according to partial response (PR), stable disease (SD), or progressive disease (PD). Pre- and post-treatment frequencies are shown for (a) total cGAS$^+$ cells, (b) cGAS$^+$ tumor cells (Calretinin$^+$), (c) cGAS$^+$ Calretinin$^-$CD8$^-$DC-LAMP$^-$ cells, and (d) cGAS$^+$ CD8$^+$ cells. Paired pre- and post-treatment comparisons within each response group were performed using Wilcoxon signed-rank tests. Changes in cell frequency, calculated as the post-treatment value minus the pre-treatment value, are shown for (e) total cGAS$^+$ cells, (f) cGAS$^+$ tumor cells, (g) cGAS$^+$ Calretinin$^-$CD8$^-$DC-LAMP$^-$ cells, and (h) cGAS$^+$ CD8$^+$ cells. P-values were adjusted using the Benjamini–Hochberg procedure to control the false discovery rate. Changes in cell frequencies were compared among the PR, SD, and PD groups using Kruskal–Wallis tests; none of these comparisons was statistically significant.

significant, no post-hoc pairwise comparisons were performed.

### Low baseline cGAS$^+$ frequency is associated with favorable progression-free survival

To test whether baseline cGAS$^+$ frequency was associated with disease outcome, we performed Kaplan–Meier survival analysis using the CutP method to define optimal thresholds. Low pre-treatment total cGAS$^+$ frequency was associated with longer PFS ($p = 0.003$) (Fig. 4**a**). Cell-compartment–specific analyses revealed that cGAS$^+$ frequency in Calretinin$^+$ tumor cells was not significantly associated with PFS ($p = 0.23$) (Fig. 4**b**). Low baseline cGAS$^+$ frequency in Calretinin$^-$CD8$^-$DC-LAMP$^-$ cells was associated with longer PFS ($p = 0.0048$) (Fig. 4**c**). Low baseline cGAS + frequency in CD8$^+$ cells was also associated with longer PFS in the CutP-based analysis ($p = 0.042$) (Fig. 4**d**).

Finally, we performed continuous univariate Cox regression analysis of baseline cGAS$^+$ frequencies. Higher total cGAS$^+$ frequency was associated with shorter PFS (HR = 1.03, 95% CI 1.01–1.06, $p = 0.018$). This association appeared mainly driven by the Calretinin$^-$CD8$^-$DC-LAMP$^-$ compartment (HR = 1.04, 95% CI 1.01–1.08, $p = 0.007$), whereas cGAS$^+$ frequency in Calretinin$^+$ tumor cells and CD8$^+$ cells was not significantly associated with PFS in continuous Cox models (Fig. 4**e**; **Table S1**).

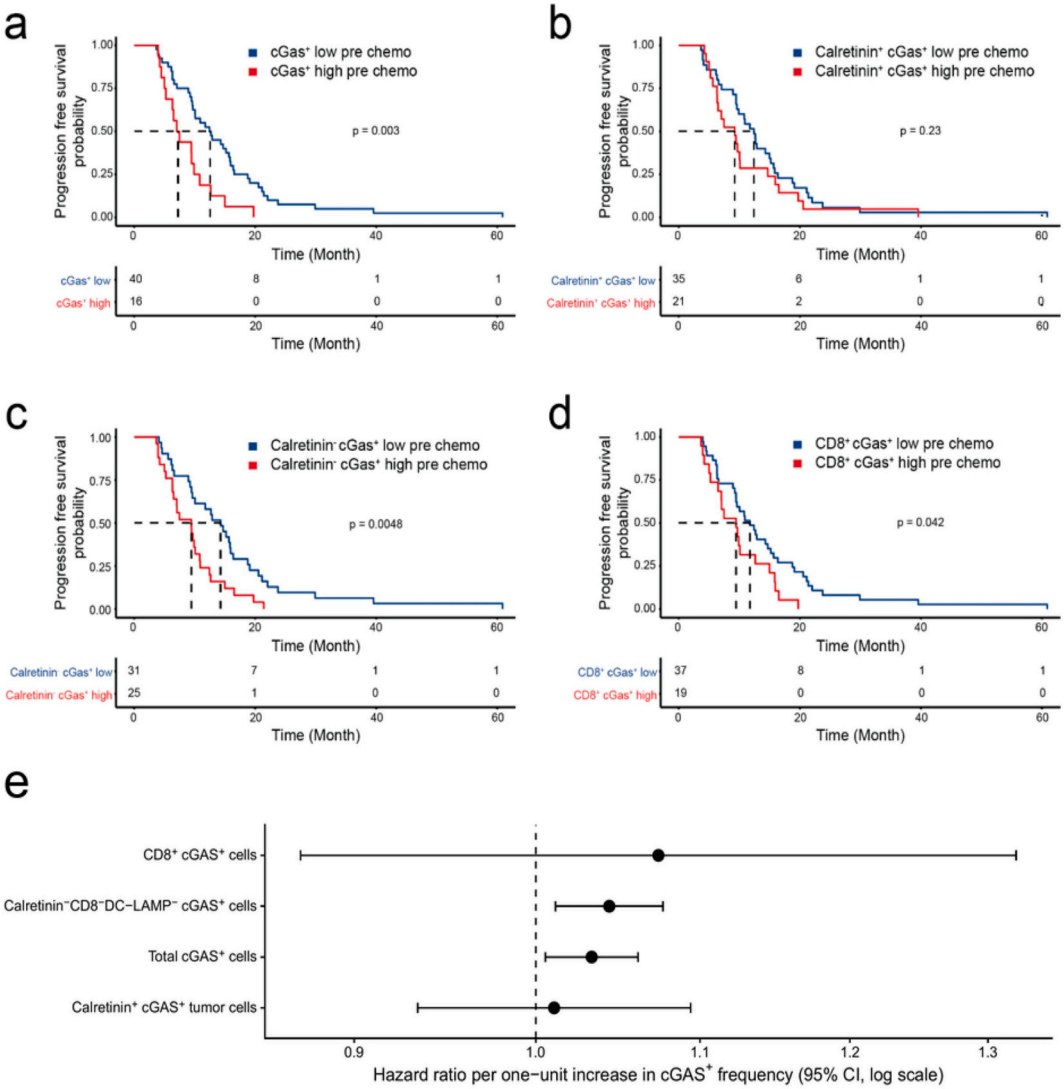


**Fig. 4.** Baseline cGAS + frequencies and progression-free survival in chemotherapy-naïve PM samples. Progression-free survival (PFS) was compared according to CutP-defined thresholds for pre-treatment cGAS + cell frequencies. Low total cGAS + frequency was associated with longer PFS (cutoff = 15.29; 71% of cases below the threshold; log-rank p = 0.003) (a). Baseline cGAS + frequency in Calretinin + tumor cells was not significantly associated with PFS (cutoff = 1.634; 62% of cases below the threshold; log-rank p = 0.23) (b). Low cGAS + frequency in Calretinin − CD8 − DC-LAMP − cells was associated with longer PFS (cutoff = 7.345; 55% of cases below the threshold; log-rank p = 0.0048) (c). Low cGAS + frequency in CD8 + cells was associated with longer PFS in the CutP-based analysis (cutoff = 0.0704; 66% of cases below the threshold; log-rank p = 0.042) (d). Univariate Cox proportional hazards models evaluating baseline cGAS + frequencies as continuous variables are shown as a forest plot (e). Hazard ratios are shown with 95% confidence intervals and correspond to a one-unit increase in cGAS + cell frequency. Cutoffs were determined using the CutP method, and survival differences in panels a–d were assessed using log-rank tests.

## Analysis in the TCGA cohort

To examine whether the tissue-level association was supported at the transcriptomic level, we analyzed CGAS/MB21D1 and STING1 expression in 86 chemotherapy-naïve PM patients from the TCGA cohort (19) with complete survival data. Using a CutP-defined threshold, low CGAS/MB21D1 transcript expression was associated with longer OS compared with high expression (cutoff = 39.4069; low, n = 19; high, n = 67; log-rank p = 0.036; Fig. S6**a**). This association was also supported when CGAS/MB21D1 expression was analyzed as a continuous variable using univariate Cox regression, with higher transcript expression associated with shorter OS (HR per one-unit increase = 1.006, 95% CI 1.001–1.010, p = 0.003).

For STING1, the CutP-defined analysis showed a survival difference between the low- and high-expression groups (cutoff = 596.951; low, n = 7; high, n = 79; log-rank p = 0.0095; Fig. S6**b**). However, this highly imbalanced stratification was not supported by continuous Cox regression (HR per one-unit increase = 1.000, 95% CI 0.9999–1.000, p = 0.30), indicating that the Kaplan–Meier result was cutpoint-dependent and should be interpreted cautiously.

## Discussion

The innate immune sensor cGAS has been widely studied in multiple malignancies and is often linked to improved survival through activation of type I interferon signaling and tumor-specific T-cell responses [18–20]. However, its role in PM remains poorly understood. We therefore investigated cGAS and STING expression in PM tumors collected before and after chemotherapy at the single-cell level. In matched pre- and post-treatment samples, chemotherapy was associated with increased $cGAS^+$ cell frequencies in $Calretinin^+$ tumor cells, $Calretinin^-CD8^-DC\text{-}LAMP^-$ cells, and $CD8^+$ cells, whereas $STING^+$ cell frequency did not differ. Within the progressive-disease subgroup, paired increases remained significant for total $cGAS^+$ cells and

Calretinin$^{-}$CD8$^{-}$DC$^{-}$LAMP$^{-}$ cells after FDR correction. These findings may reflect stronger treatment-associated cGAS induction in tumors with resistant disease. However, because the magnitude of the pre- to post-treatment change did not differ significantly among the PR, SD, and PD groups (Fig. 3**e–h**), the subgroup findings should not be interpreted as evidence of a response-specific effect. Low baseline total cGAS$^{+}$ frequency and cGAS$^{+}$ frequency in the Calretinin$^{-}$CD8$^{-}$DC-LAMP$^{-}$ compartment were associated with longer PFS. In several cancers, including colorectal, breast, and lung, cGAS/STING activation has been associated with enhanced anti-tumor immunity and improved outcomes [18–20]. Furthermore, activation of STING in preclinical mouse models led to potent therapeutic effects and tumor regression in a STING-dependent manner [21]. In contrast, our data in PM reveal that high cGAS expression correlates with poor prognosis, suggesting a context-dependent, pro-tumorigenic role. At the transcriptomic level, analysis of the TCGA cohort showed a concordant association between higher CGAS/MB21D1 mRNA expression and shorter OS. However, this analysis was based on bulk transcript expression, whereas the primary cohort assessed protein-positive cell frequencies in marker-defined tissue compartments; the two analyses should therefore be considered complementary rather than directly equivalent. Continuous STING1 transcript expression was not associated with OS.

PM is characterized by chronic asbestos-induced inflammation, in which persistent DNA damage and extracellular HMGB1 can activate cGAS [22–24]. Chronic activation of innate immune pathways is a hallmark of cancer and can promote tumorigenesis and progression [22,23]. Carcinogenesis driven by chronic inflammation may also be mediated through STING [25]. Consistent with this, patients with high HMGB1 serum levels exhibit shorter survival [26], aligning with our observation that high baseline cGAS correlates with poor PFS.

A limitation of our multiplex panel is that CD8 was not combined with CD3, and therefore CD8$^{+}$ events are referred to as CD8$^{+}$ cells rather than definitive CD8$^{+}$ T cells. Similarly, DC-LAMP$^{+}$ cells were not co-stained with lineage markers such as CD11c or HLA-DR. The Calretinin$^{-}$CD8$^{-}$DC-LAMP$^{-}$ compartment should therefore be interpreted as an unclassified non-tumor compartment rather than a defined stromal population. Consequently, the strongest conclusions of this study relate to Calretinin$^{+}$ tumor cells and to broad cGAS expression patterns across marker-defined compartments, rather than to fully resolved immune or stromal cell subsets. While our study does not provide functional evidence (neither *in vitro* nor *in vivo*) that cGAS drives mesothelioma aggressiveness or treatment resistance, several previously described studies highlight potential tumor-promoting effects of cGAS/STING. Chronic cGAS/STING signaling has been shown to drive immunosuppressive microenvironments by inducing PD-L1 and IDO expression, recruiting myeloid-derived suppressor cells (MDSCs), and enhancing regulatory T cell infiltration [27,28]. Such mechanisms are particularly relevant to PM, a tumor with low antigenicity and high infiltration of regulatory immune cells [29]. A similar survival benefit of low cGAS mRNA expression in chemotherapy-naïve samples has been reported in colorectal carcinoma [30].

Another potential tumor-promoting mechanism involves the interaction of cGAS with PARP1, which suppresses homologous recombination-mediated repair, thereby promoting genomic instability and tumor growth [13]. Although tumor cell cGAS$^{+}$ frequency was not associated with PFS in the continuous Cox model, asbestos fibers exacerbate DNA damage [31], and high cGAS in chemotherapy-naïve PM may reflect impaired DNA repair and more aggressive tumor biology. In addition, cGAS/STING-mediated activation of TBK1 can inhibit AMPK, thereby blocking autophagy, a tumor-suppressive mechanism [32]. Inhibition of TBK1 in breast cancer cells restores autophagy and induces tumor cell death [33], and TBK1 suppression is known to promote apoptosis via NF-κB signaling [34]. These findings provide a further potential explanation for the association between lower cGAS expression and better outcome.

The role of cGAS/STING in tumor-associated CD8$^{+}$ cells remains under active investigation [39]. While cGAS has been reported to support CD8$^{+}$ T cell stemness and enhance tumor control [35], cGAS$^{+}$ frequency in CD8$^{+}$ cells was not associated with PFS in the continuous Cox model, and changes in this compartment did not differ significantly among response groups. The continuous association with PFS was strongest in the Calretinin$^{-}$CD8$^{-}$DC-LAMP$^{-}$ compartment. However, because this compartment was not resolved using dedicated lineage markers and the present study is observational, these findings do not establish this population as a causal driver of tumor progression or treatment resistance. Although compartment-specific roles of stromal cGAS have been reported in other tumor models [38], the present panel does not permit classification of this population as stromal.

In conclusion, low baseline total cGAS$^{+}$ frequency and cGAS$^{+}$ frequency in the Calretinin$^{-}$CD8$^{-}$DC-LAMP$^{-}$ compartment were associated with longer PFS in PM. However, changes in cGAS$^{+}$ frequency did not differ significantly among chemotherapy-response groups. Our findings therefore support further evaluation of cGAS as a candidate prognostic biomarker in PM. Further studies using lineage-resolved panels and functional models are required to define the compartment-specific roles of cGAS/STING in PM.

Declarations.

Ethics approval and consent to participate.

All patients gave informed, written consent and the study was conducted in accordance with the declaration of Helsinki. Samples were collected at the University Hospital Zurich between 1999 and 2009. Part of the study was approved by the Institutional Ethical Review Board of the Canton of Zurich under reference number EK-ZH 2020–02566. This study was conducted between 2022 and 2024.

## CRediT authorship contribution statement

**Antoine Torchiat:** Writing – review & editing, Methodology, Investigation, Formal analysis, Data curation. **Karina Silina:** Writing – review & editing, Methodology, Investigation, Formal analysis, Data curation, Conceptualization. **Arya Ashok Nair:** Methodology, Formal analysis, Data curation. **Laura Viktoria Heeb:** Supervision, Formal analysis. **Isabelle Opitz:** Resources, Conceptualization. **Anurag Gupta:** Writing – review & editing, Writing – original draft, Methodology, Investigation, Formal analysis, Conceptualization. **Alessandra Curioni-Fontecedro:** Writing – review & editing, Writing – original draft, Supervision, Funding acquisition, Conceptualization.

## Declaration of competing interest

The authors declare that they have no known competing financial interests or personal relationships that could have appeared to influence the work reported in this paper.

## Acknowledgments

This work was supported by the Stiftung für angewandte Krebsforschung Zürich, Switzerland; University Research pool grant from the University of Fribourg, Switzerland; Research Grants from Kanton Hospital of Fribourg, Switzerland. We thank Michal Beffinger and Essence Omics for biostatistical and bioinformatic support, including assistance with the TCGA analyses.

## Appendix A. Supplementary data

Supplementary data to this article can be found online at https://doi.org/10.1016/j.lungcan.2026.109553.

## References


[1] S. Hiltbrunner, L. Mannarino, M.B. Kirschner, I. Opitz, A. Rigutto, A. Laure, et al., Tumor Immune Microenvironment and Genetic Alterations in Mesothelioma, Front. Oncol. 11 (2021) 660039.

[2] P.M. Forde, A. Scherpereel, A.S. Tsao, Use of Immune Checkpoint Inhibitors in Mesothelioma, Curr. Treat. Options Oncol. 20 (2) (2019) 18.

[3] P. Baas, A. Scherpereel, A.K. Nowak, N. Fujimoto, S. Peters, A.S. Tsao, et al., First-line nivolumab plus ipilimumab in unresectable malignant pleural mesothelioma (CheckMate 743): a multicentre, randomised, open-label, phase 3 trial, Lancet 397 (10272) (2021) 375–386.

[4] X. Tan, L. Sun, J. Chen, Z.J. Chen, Detection of Microbial Infections through Innate Immune Sensing of Nucleic Acids, Annu. Rev. Microbiol. 72 (2018) 447–478.

[5] M. Motwani, S. Pesiridis, K.A. Fitzgerald, DNA sensing by the cGAS-STING pathway in health and disease, Nat. Rev. Genet. 20 (11) (2019) 657–674.

[6] L. Deng, H. Liang, M. Xu, X. Yang, B. Burnette, A. Arina, et al., STING-Dependent Cytosolic DNA Sensing Promotes Radiation-Induced Type I Interferon-Dependent Antitumor Immunity in Immunogenic Tumors, Immunity 41 (5) (2014) 843–852.

[7] S.R. Woo, M.B. Fuertes, L. Corrales, S. Spranger, M.J. Furdyna, M.Y. Leung, et al., STING-dependent cytosolic DNA sensing mediates innate immune recognition of immunogenic tumors, Immunity 41 (5) (2014) 830–842.

[8] L. Schadt, C. Sparano, N.A. Schweiger, K. Silina, V. Cecconi, G. Lucchiari, et al., Cancer-Cell-Intrinsic cGAS Expression Mediates Tumor Immunogenicity, Cell Rep. 29 (5) (2019) 1236–48 e7.

[9] H. Liang, L. Deng, Y. Hou, X. Meng, X. Huang, E. Rao, et al., Host STING-dependent MDSC mobilization drives extrinsic radiation resistance, Nat. Commun. 8 (1) (2017) 1736.

[10] S.F. Bakhoum, B. Ngo, A.M. Laughney, J.A. Cavallo, C.J. Murphy, P. Ly, et al., Chromosomal instability drives metastasis through a cytosolic DNA response, Nature 553 (7689) (2018) 467–472.

[11] H. Cheng, Q. Xu, X. Lu, H. Yuan, T. Li, Y. Zhang, et al., Activation of STING by cGAMP Regulates MDSCs to Suppress Tumor Metastasis via reversing Epithelial-Mesenchymal transition, Front. Oncol. 10 (2020) 896.

[12] F.R. Liu, M.J. Jiang, Z. Mei, C.J. Lin, L. Tian, cGAS-STING signalings potentiate tumor progression via sustaining cancer stemness, Transl. Oncol. 20 (2022) 101404.

[13] H. Liu, H. Zhang, X. Wu, D. Ma, J. Wu, L. Wang, et al., Nuclear cGAS suppresses DNA repair and promotes tumorigenesis, Nature 563 (7729) (2018) 131–136.

[14] P. Tallon de Lara, V. Cecconi, S. Hiltbrunner, H. Yagita, M. Friess, B. Bode, et al., Gemcitabine Synergizes with Immune Checkpoint Inhibitors and Overcomes Resistance in a Preclinical Model and Mesothelioma patients, Clin. Cancer Res. 24 (24) (2018) 6345–6354.

[15] C. Contal, O'Quigley JJCs, analysis d, An Application of Changepoint Methods in Studying the Effect of Age on Survival in Breast Cancer. 30 (3) (1999) 253–270.

[16] M. Ogluszka, M. Orzechowska, D. Jedroszka, P. Witas, A.K. Bednarek, Evaluate Cutpoints: Adaptable continuous data distribution system for determining survival in Kaplan-Meier estimator, Comput. Methods Programs Biomed. 177 (2019) 133–139.

[17] , Therneau TM, editor Extending the Cox model. Proceedings of the first Seattle symposium in biostatistics: survival analysis; 1997: Springer.

[18] T. Xia, H. Konno, J. Ahn, G.N. Barber, Deregulation of STING Signaling in Colorectal Carcinoma Constrains DNA damage responses and Correlates with Tumorigenesis, Cell Rep. 14 (2) (2016) 282–297.

[19] L. Wu, J. Cao, W.L. Cai, S.M. Lang, J.R. Horton, D.J. Jansen, et al., KDM5 histone demethylases repress immune response via suppression of STING, PLoS Biol. 16 (8) (2018) e2006134.

[20] S. Kitajima, E. Ivanova, S. Guo, R. Yoshida, M. Campisi, S.K. Sundararaman, et al., Suppression of STING Associated with LKB1 loss in KRAS-Driven Lung Cancer, Cancer Discov. 9 (1) (2019) 34–45.

[21] L. Corrales, L.H. Glickman, S.M. McWhirter, D.B. Kanne, K.E. Sivick, G.E. Katibah, et al., Direct Activation of STING in the Tumor Microenvironment leads to Potent and Systemic Tumor Regression and Immunity, Cell Rep. 11 (7) (2015) 1018–1030.

[22] D. Hanahan, R.A. Weinberg, Hallmarks of cancer: the next generation, Cell 144 (5) (2011) 646–674.

[23] S. Jube, Z.S. Rivera, M.E. Bianchi, A. Powers, E. Wang, I. Pagano, et al., Cancer cell secretion of the DAMP protein HMGB1 supports progression in malignant mesothelioma, Cancer Res. 72 (13) (2012) 3290–3301.

[24] L. Andreeva, B. Hiller, D. Kostrewa, C. Lassig, C.C. de Oliveira Mann, D. Jan Drexler, et al., cGAS senses long and HMGB/TFAM-bound U-turn DNA by forming protein-DNA ladders, Nature 549 (7672) (2017) 394–398.

[25] J. Ahn, T. Xia, H. Konno, K. Konno, P. Ruiz, G.N. Barber, Inflammation-driven carcinogenesis is mediated through STING, Nat. Commun. 5 (2014) 5166.

[26] C. Tabata, S. Kanemura, R. Tabata, E. Masachika, E. Shibata, T. Otsuki, et al., Serum HMGB1 as a diagnostic marker for malignant peritoneal mesothelioma, J. Clin. Gastroenterol. 47 (8) (2013) 684–688.

[27] D. Liang, H. Xiao-Feng, D. Guan-Jun, H. Er-Ling, C. Sheng, W. Ting-Ting, et al., Activated STING enhances Tregs infiltration in the HPV-related carcinogenesis of tongue squamous cells via the c-jun/CCL22 signal, Biochim. Biophys. Acta 1852 (11) (2015) 2494–2503.

[28] H. Lemos, E. Mohamed, L. Huang, R. Ou, G. Pacholczyk, A.S. Arbab, et al., STING Promotes the growth of Tumors Characterized by Low Antigenicity via IDO Activation, Cancer Res. 76 (8) (2016) 2076–2081.

[29] A. Decout, J.D. Katz, S. Venkatraman, A. Ablasser, The cGAS-STING pathway as a therapeutic target in inflammatory diseases, Nat. Rev. Immunol. 21 (9) (2021) 548–569.

[30] X. An, Y. Zhu, T. Zheng, G. Wang, M. Zhang, J. Li, et al., An Analysis of the Expression and Association with Immune Cell Infiltration of the cGAS/STING Pathway in Pan-Cancer, Mol. Ther. Nucleic Acids 14 (2019) 80–89.

[31] N. Choe, S. Tanaka, E. Kagan, Asbestos fibers and interleukin-1 upregulate the formation of reactive nitrogen species in rat pleural mesothelial cells, Am. J. Respir. Cell Mol. Biol. 19 (2) (1998) 226–236.

[32] J. Nassour, R. Radford, A. Correia, J.M. Fuste, B. Schoell, A. Jauch, et al., Autophagic cell death restricts chromosomal instability during replicative crisis, Nature 565 (7741) (2019) 659–663.

[33] L.C. Liu, Y.C. Shen, Y.L. Wang, W.R. Wu, L.C. Chang, Y.H. Chen, et al., Growth-promoting function of the cGAS-STING pathway in triple-negative breast cancer cells, Front. Oncol. 12 (2022) 851795.

[34] D.A. Barbie, P. Tamayo, J.S. Boehm, S.Y. Kim, S.E. Moody, I.F. Dunn, et al., Systematic RNA interference reveals that oncogenic KRAS-driven cancers require TBK1, Nature 462 (7269) (2009) 108–112.

[35] W. Li, L. Lu, J. Lu, X. Wang, C. Yang, J. Jin, et al., cGAS-STING-mediated DNA sensing maintains CD8(+) T cell stemness and promotes antitumor T cell therapy, Sci. Transl. Med. 12 (549) (2020).